Capillary penetration in fibrous matrices studied by dynamic spiral magnetic resonance imaging

Atsushi Takahashi,[1] Mats Häggkvist,[2] and Tie-Qiang Li[3,*]
[1]*Stanford University School of Medicine, Lucas MRS Center, Room P-272, Stanford, California 94305-5488*
[2]*Swedish Pulp and Paper Research Institute, P.O. Box 5604, S-114 86 Stockholm, Sweden*
[3]*Karolinska MR Research Center, Building N8, S-171 76 Stockholm, Sweden*
(Received 3 December 1996; revised manuscript received 28 April 1997)

The dynamic spiral nuclear magnetic resonance (NMR) imaging technique was used to investigate the water imbibition into cellulose fiber matrices. The advancing water boundary, water concentration distribution, and swelling degree within the fiber matrix samples were monitored as a function of time over the entire absorption process. A combined image that shows the time evolution of the absorbed water concentration distribution within the fiber matrix was synthesized from the dynamically acquired NMR image data set. The NMR imaging data clearly demonstrated that water imbibition into a fiber matrix consists of two different processes: water penetration into capillaries between fibers and water diffusion into the cellulose fibers. The advancing liquid front is primarily determined by the water capillary flow and can be quantitatively described by Washburn equation. The slower water diffusion process in fibers is mainly responsible for the fiber swelling. The time evolution of the absorbed water concentration distribution can be qualitatively interpreted in terms of steady capillary flow and concentration-gradient-driven diffusion into fibers with a constant permeability. The effects of pore morphology, tortuosity, and surface heterogeneity to the water absorption process are also discussed. [S1063-651X(97)15708-7]

PACS number(s): 47.55.Mh, 47.90.+a, 76.60.Pc

INTRODUCTION

Solvent diffusion into polymeric materials in general [1–3] and water penetration into fibrous matrices in particular [4–6] have been extensively investigated. The molecular dynamics and thermodynamic properties of the mobile molecules are known to be modified when they are confined between macromolecules [2]. Porous polymer materials are often found in applications where the transportation through spatial restrictions is important. Understanding these processes is therefore fundamentally important to the new developments in such diverse fields as biomedicine, chemical engineering, textile, and the petroleum industry. For example, water penetration in fibrous matrices is an important aspect for printing processes, surface sizing, and the control of paper coating. The quality of many fiber products, such as diapers, sanitary pads, and incontinence systems, is also essentially influenced by water absorption capacity and the spreading speed of the water phase into the fiber matrix. The successful control of water penetration in industrial fiber products requires the knowledge of the absorption determining factors of the fiber matrix.

Various methods to measure water absorption in fiber matrix have been proposed in the literature [7–15]. With these methods, the liquid transport into a fiber matrix is monitored by the physical changes, such as weight, fluorescence, reflectance, transmittance, electrical conductivity, etc. For example, the Bristow method [15], which measures the transferred liquid volumes as a function of the contact time, is widely used to determine the absorption coefficient and the wetting delay during short time intervals. Different techniques such as microscopy and Wihelmy dynamic contact angle measurement [16] have been applied to characterize the local structure and surface changes of individual fibers caused by liquid wetting. However, none of these methods can simultaneously provide information both on the absorption kinetics and the microstructure changes within a fiber matrix. Two types of experiments [17–22] have been used to study the kinetics of the water absorption process: unidirectional penetration from a large liquid reservoir into a fiber matrix and penetration of a finite liquid drop deposited on the fibrous assembly. The results obtained from these two types of systems cannot be directly compared and have given rise to some confusions about the fundamental understanding of water absorption in a fiber matrix. Unidirectional penetration of water into a fiber matrix clearly demonstrates that the kinetics of the process follows Washburn equation [23,24], whereas the kinetics of radial penetration of a finite liquid drop into a fabric does not follow any hitherto known theoretical predication. In a porous medium such as a fiber matrix with a nonuniform pore size distribution and a wide variety of pore microgeometry, the local capillary driving force is likely to be highly heterogeneous. When the amount of liquid is limited as in a finite drop penetration experiment, besides the initial imbibition there might be liquid redistribution processes involved between the pores of different sizes and microgeometry.

Although the advancement of a liquid boundary in an unidirectional penetration experiment with unlimited water reservoir can be well described by Washburn equation, several simplifications are made. For example, the interfacial contact angle is assumed to be constant and the pore morphology is simplified to an equivalent cylindrical pore radius. In reality, the microscopic variations in chemical composition, discontinuity, and roughness of the fiber surfaces are likely to be responsible for dynamic contact angle hysteresis. The pore morphology in a fiber matrix is even more complex. Pores

*Author to whom correspondence should be addressed.

have a wide variety of shape, size, connectivity, and wall continuity. In a saturated fiber matrix, there are void spaces occupied by water that might not participate in active flow transportation due to mechanical obstructions such as isolated or dead-end pores. In addition to water trapped in the lamella slits within the cell wall, in the lumen, and the pits, the arrangement of fibers in a fiber assembly can also create a large amount of dead-end pores or stagnant regions which are less likely to participate in the liquid flow. This is probably one of the main reasons why the pressure drop for flow in fibrous structures is very high while the porosity of the fiber webs is typically not low. It remains to clarify whether it is adequate to approximate such a complex pore morphology as in a fiber matrix by an effective cylindrical pore radius.

There might be many driving potentials involved in liquid transport in porous materials, such as capillary pressure, external pressure, vapor pressure, concentration gradient, and temperature gradient. Besides capillary flow in the pores as described by the Washburn equation, diffusion transport within the fibers might also be a very important mechanism. For example, it has been reported that in sized paper sheets the liquid front advances in proportion to the contact time and it had been postulated that diffusion within the fibers is the primary transport mechanism [9]. There are even hypotheses [12,13] that the surface adsorption of the vapor phase onto fiber surface taking place ahead of the advancing liquid boundary might also be an important mechanism for water transport in fiber matrices. However, the complexity of the system and the lack of experimental techniques to provide both kinetic and structural information within the fiber matrix have hampered attempts to clarify the role of diffusion and surface adsorption in water imbibition into a fiber matrix. The primary objective of this investigation is to try to clarify some of these fundamental aspects of water transport mechanisms in fiber matrices. For this purpose we have used the dynamic spiral NMR imaging technique which can rapidly monitor both concentration and structural changes within a fiber matrix as a function of time.

In the last few years, NMR imaging has been recognized as a powerful tool for studying diffusion of solvents into polymeric materials [25–31]. NMR images can provide both qualitative and quantitative information to reveal the fundamental aspects of the transport mechanism within the materials. The pixel intensity of a NMR image is not only dependent on the local concentration of the nuclear spins, but also their T_1 and T_2 NMR relaxation times and self-diffusion coefficient. It is possible to enhance the NMR relaxation or diffusion contrasts by appropriately adjusting the time parameters in the imaging pulse sequence. The rich information content of NMR spectroscopy combined with spatial resolution should make it possible to study different properties of the polymer matrix, such as polarity, degree of cross-linking, and porosity, which greatly influence solvent penetration. Up to now the NMR imaging method has been used as a noninvasive tool to monitor the diffusion boundary of the mobile components within a polymeric material. By means of this technique, different types of diffusion processes such as the case II and the Fickian diffusion processes can be routinely identified [32,33]. Furthermore, the correlation between the diffusion behavior and structure characteristics such as the degree of cross-linking can also be studied [34]. Recently, NMR imaging based on radio frequency field gradients [35] has been used for studying solvent penetration in polymers to overcome the magnetic susceptibility artifacts and the limitation of the short NMR transverse relaxation time, T_2.

In order to provide accurate dynamic image data without flow distortions, it is critical that the total experiment time to produce an image in relation to the diffusion process itself has to be short. In this study the rapid spiral NMR imaging technique is used to measure the spatial distribution of the water proton concentration within the fiber matrix and to monitor the structural changes within the fiber matrix during the water imbibition. Spiral imaging is one of the most rapid NMR imaging techniques in the category of the gradient recalled echo method. The advantages of the spiral imaging technique rest with the fact that without stringent requirements for the amplitude and slew rate of the gradient system, during a few free-induction decays, a set of k space data can be collected sufficiently dense and extensive for reconstructing an image [36–38]. Furthermore, it has been demonstrated that spiral imaging is less sensitive to distortion and ghosting artifacts from flowing material [38], since the first- and higher-order moments of the spiral readout gradients are zero at the origin of k-space and increase only slowly and smoothly with k-space position. In the present study, we used a pulse sequence based on the combination of a self-refocused rf pulse [39–41] with spiral readout gradients. This shortens both the spin-echo time and pulse sequence repetition time, since the self-refocused rf pulse dephases the existing transverse magnetization while it excites the longitudinal component.

EXPERIMENT

A never dried and fully bleached softwood sulfate wood pulp (Imperial Anchor, Iggesund AB, Sweden) was used for the study. A dilute pulp suspension (about 0.5 wt %) was prepared using the pulp and de-ionized water. Four cellulose fiber cylinders were prepared from this pulp suspension by using a Plexiglas jar (95×150 mm^2) with a filter at the bottom. The wet fiber plugs were dried at 105 °C for 24 h. There was no significant distortion in the cylindrical shape of the fiber plug after drying. The densities for the dried fiber plugs were determined from the measured volume and weight. The porosity was evaluated by assuming that the density of the cellulose fiber was 1.55 g/cm^3. The size, weight, density, and porosity for these fiber plugs are listed in Table I.

All the NMR imaging experiments were performed by using a 1.5-T whole body medical scanner (GE Signa). The NMR imaging raw data were collected by using a dynamic spiral pulse sequence, which is schematically presented in Fig. 1. As shown, the slice selection was achieved by an amplitude modulated band selective 90° rf pulse with uniform response and pure phase. The selected slice thickness was 5 mm, and the corresponding rf pulse duration is 3.2 ms with a selective bandwidth of 1.25 kHz. The selective rf pulse was designed to focus the transverse magnetization along the real axis in the rotating reference frame. The system hardware had a gradient slew rate and gradient amplitude limits of 17 mT/m ms and 10 mT/m, respectively. The design of the interleaved spiral readout gradients was based

TABLE I. Cellulose fiber plugs used for NMR imaging experiments.

Sample	Height (mm)	Diameter (mm)	Dry weight (g)	Wet weight (g)	Density (g/cm^3)	Porosity (%)
1	104.7	93.5	172	990	0.178	88.5
2	104.5	93.8	176	1012	0.181	88.3
3	139.0	94.1	172	998	0.176	88.6
4	137.8	92.2	166	955	0.180	88.4

on the variable rate method proposed by Hardy and Cline [42]. The desired in-plane spatial resolution is 0.84 mm/pixel. Five turns of the spiral trajectory could be achieved with a readout window of 19.2 ms, yielding a field of view of 215 mm in 20 interleaves. The first 7.3 ms of the wave forms were limited by the maximum slew-rate constraint, whereas the remainder were limited by the gradient amplitude constraint. The constant gradient amplitude portion of the spiral wave forms produces a relatively uniform sampling density function and, therefore, some correction was required for only the slew-rate limited portion. At the end of the spiral readout gradient, trapezoidal spoiler gradients of constant amplitude were applied. Each interleave was realized by rotating the basic wave forms of the readout gradients around the slice selection axis using the scanner's wave form rotation hardware. The actual *k*-space trajectory was measured using a self-encoding technique [43]. With a sequence repetition time of 50 ms, a temporal resolution of one image per second was achieved. The pulse sequence essentially takes a snapshot of the instantaneous water distribution and reduces the sensitivity of the image intensity to artifacts arising from water diffusion. In a rapid spiral imaging experiment, the time to acquire an image data set is short compared to the water absorption process and the influence of the advancing water boundary on the NMR signal is negligible during a spiral image data sampling.

After the bottom of a fiber plug was set in contact with the water reservoir, 128 axial images were collected successively for each sample to monitor the water imbibition in the vertical direction. In order to approach a steady-state transverse magnetization, five dummy scans were performed ahead of each image data sampling. The water used for the absorption experiment was doped with $MnCl_2$ to reduce the NMR T_1 relaxation time of the water protons and allow speedy data sampling. The effective T_2 and T_1 are approximately 90 and 200 ms, respectively. There is a 3 s waiting time after each image data sampling, and so the total NMR experimental time for each sample is 544 s. The image plane was selected to pass through the central axis of the fiber plug. The volume of the water resource was sufficiently large so that the change of water level during NMR imaging experiment was negligible. The image reconstruction was performed off line using a Sparc-5 Sun workstation using the method outlined by Meyer *et al.* [44]. To compensate for the nonuniform *k*-space sampling density a nonlinear weighting was applied to the raw data and a gridding procedure was then used to convolve the data sampled in spiral trajectories onto a two-dimensional (2D) square matrix. Finally, a 2D fast Fourier transformation (FFT) was performed to produce a 256×256 image. The complex image was divided by the Fourier transformation of the gridding kernel to correct the image intensity modulation caused by the convolution. The reconstructed images were analyzed by using MATLAB (The Math Work Inc.) software. The advancing water boundary was determined by using a maximum gradient edge detection method.

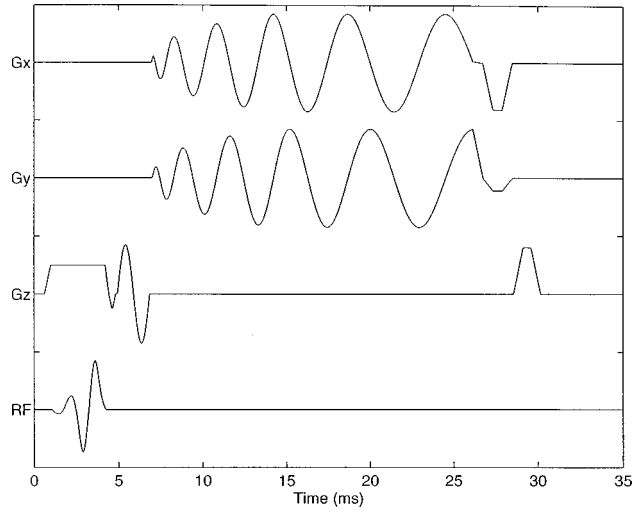

FIG. 1. Spiral phase contrast pulse sequence. The slice selection is achieved using a delayed self-refocus pulse and is immediately followed by a bipolar flow encoding gradient pulse. The flow encoding can be switched on and off or inverted between measurements and can be applied along any direction of interest. The readout gradient wave form produces a spiral trajectory in *k* space.

RESULTS AND DISCUSSION

Figure 2 shows a set of amplitude NMR images of a fiber matrix in the transverse plane. These images were acquired as a function of time by using the dynamic spiral pulse sequence after the fiber matrix was brought into contact with the water reservoir. Since the NMR imaging experiment was performed under steady-state conditions, the contribution from NMR relaxation time and molecular self-diffusion can be approximately regarded as constant [45]. The pixel intensities in these images are, therefore, approximately proportional to the water proton density. As shown in Fig. 2, the advancing water front reflects approximately the outline of the selected slice. This indicates that the cellulose fiber network is at large macroscopically homogeneous and the water penetration in the fiber matrix appears to occur in a quasi-steady manner with a reasonably sharp advancing liquid front despite the complicated microscopic pore structure.

The time-domain NMR signal observed in an interleaved spiral experimental is essentially a free induction decay, and blurring artifacts arising from magnetic susceptibility varia-

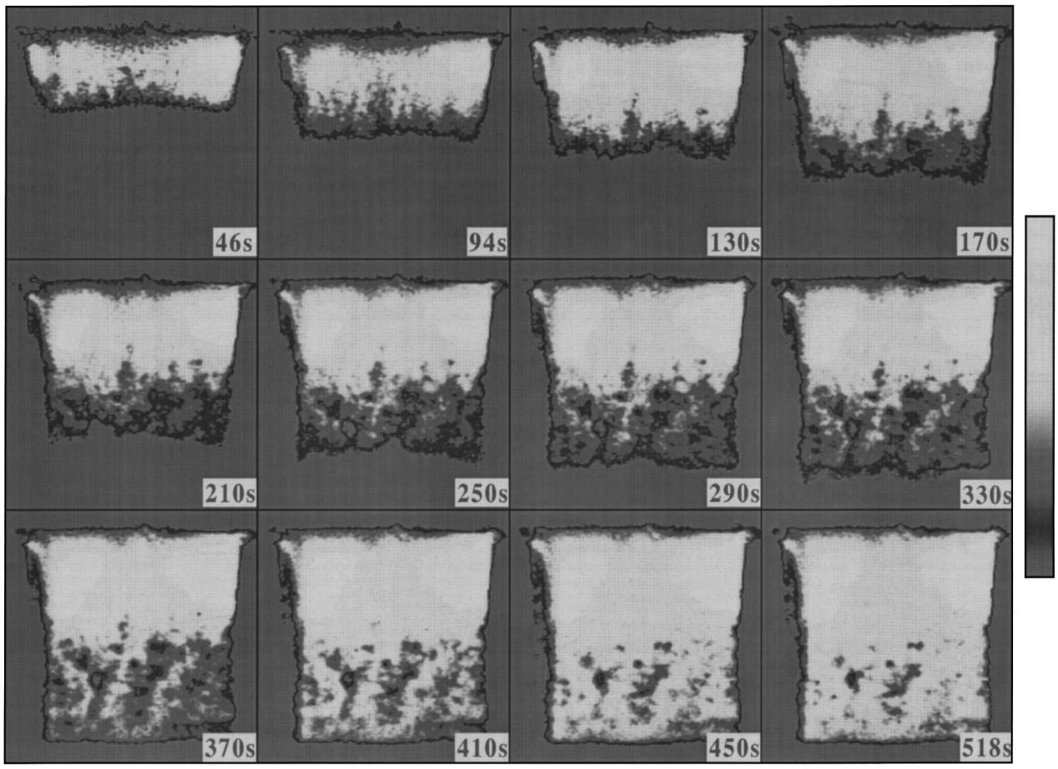

FIG. 2. Spin density distribution images at different contact times recorded by using the dynamic spiral NMR imaging technique. The images are inverted and the water front advances downwards from the top.

tions could be problematic. Particularly, the intensity artifacts might be significant at the leading edge of the advancing liquid front where four phases (air, water, dry, and wet fibers) meet. In order to reduce the effects of the susceptibility artifacts, spatial averaging was performed in the quantitative analysis of the water concentration profile. The average water concentration profile in a fiber matrix along the direction transverse to the water diffusion direction at a certain experimental time was obtained by summing up the rows of the corresponding NMR image. By sequentially combining all the 128 concentration profiles into a single matrix, a synthesized image exhibiting the time evolution of the water concentration distribution in a fiber matrix was obtained. Figure 3 demonstrates such an example. Applying the Sobel gradient edge detection algorithm to the synthesized image, the time evolution curves for the water concentration gradients were obtained (Fig. 4).

As clearly shown in Fig. 4, the development of the water concentration gradient follows two different time courses, indicating two different water penetration processes. This is in accordance with the direct visual observations of the individual NMR spin density images shown in Fig. 2. As the

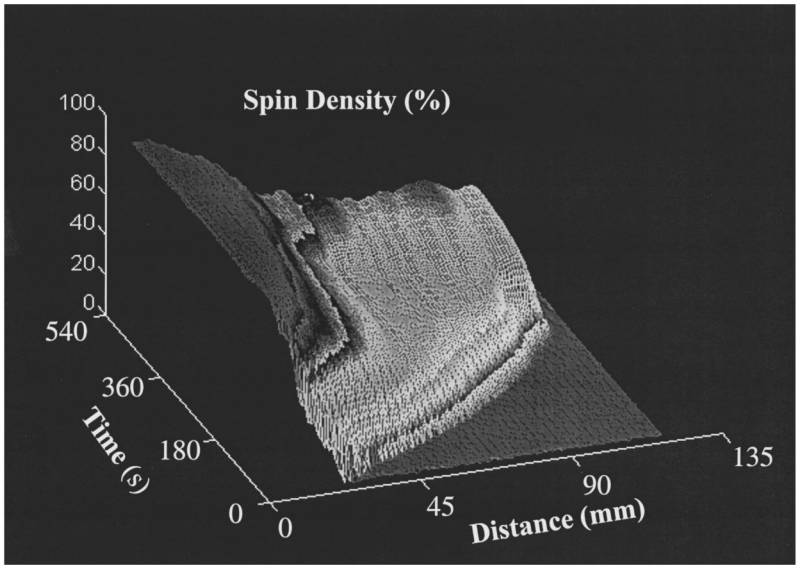

FIG. 3. Liquid saturation profile as a function of contact time and distance from the contacting liquid surfaces.

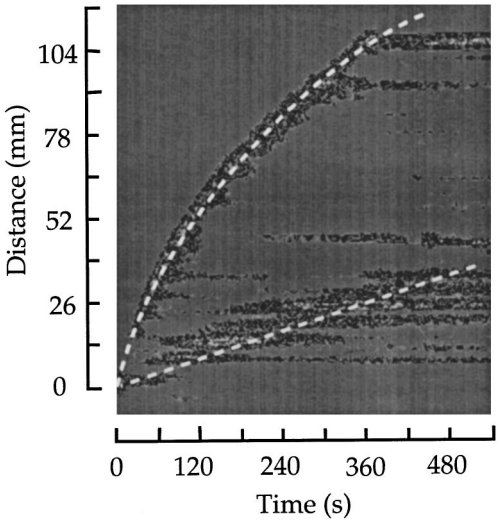

FIG. 4. Advancing liquid front as a function of time as evaluated from the gradient of the concentration distribution. The curve represents the best nonlinear curve fitting of Eq. (2) to the data.

water front progresses with time, the NMR image data indicate that the water imbibition was separated into two regions: a front region with straight vertical outer boundaries as the dry fiber matrix and a region with distorted vertical boundaries. The original dry fiber plug is a nearly perfect cylinder. This implies that the region with distorted vertical boundaries is apparently related to different degrees of fiber swelling. Although NMR imaging cannot resolve individual fibers, fiber matrix expansion gives direct evidence of fiber swelling due to intrafiber water diffusion. The front region with unchanged vertical boundaries exhibited a lower and imhomogeneous water concentration distribution. This is most attributable to water penetration in the interfiber capillary pores, which resulted in insignificant fiber swelling. The distance between these two regions increases with time, indicating that the capillary penetration and intrafiber diffusion follow different time courses. The intrafiber water diffusion is apparently a slower process, since there must exist water surrounding the fibers due to capillary flow before the concentration-gradient-controlled diffusion process could start. Furthermore, the intrafiber water diffusion is greatly influenced by the permeability and crystallinity of the fiber cell wall.

When the pressure drop due to air transport and inertial effects are negligible, the liquid penetration into an open pore of constant pore radius r is determined by the balance between the capillary pressure and the pressure drop due to liquid flow [23,24],

$$dh/dt = R^2/8\eta h(2\gamma_{LV}\cos\theta/R - \rho g h), \qquad (1)$$

where dh/dt is the rate of fluid rising in a open capillary and g is the gravity constant. The liquid viscosity, surface tension, density, and contact angle are represented by η, γ_{LV}, ρ, and θ, respectively. Equation (1) is known as the Washburn equation, which describes the rate of fluid rise in a vertical capillary. If the contact angle is assumed to be constant, Eq. (1) can be readily solved,

$$\ln[h_\infty/(h_\infty - h)]h = R^2\rho g t/8\eta, \qquad (2)$$

where $h_\infty = 2\gamma_{LV}\cos\theta_e/R\rho g$ is the equilibrium liquid height that can be achieved in a vertical capillary by letting $dh/dt = 0$ and $\theta = \theta_e$ at $t = \infty$. The curve shown in Fig. 4 represents the best nonlinear curve fitting of Eq. (2) to the time course of the advancing water front as measured by NMR imaging. The fitting is quite good, and this gives further support that the advancing water front resulting in insignificant fiber matrix swelling is most likely due to water flow into capillary pores between the cellulose fibers. From the curve fitting results, the capillary radius R was estimated to be 4.3 ± 0.5 μm. The complex pore structure in a fiber matrix is certainly not a circular cylinder of constant cross section as it is assumed in the Washburn equation. The pore radius estimated from the water absorption experiments can only be regarded as the effective pore radius. The mean pore radius for cellulose fiber materials without fillers is typically a few μm irrespective of the experimental techniques used to measure it. Wood pulp cellulose fibers are partly flat natural fibers with large variations in the dimensions. This is also one of the reasons why the pores in a cellulose fiber matrix have a wide variety of shape, size, and connectivity. There are different definitions for the mean pore radius of a fiber assembly depending on the experimental methods used to characterize it [6,17–22]. The effective pore radius obtained from liquid penetration experiments serves as a simple means to characterize this aspect of porous fiber matrices.

Another parameter obtainable from the curve fitting procedure is h_∞, which is estimated to be 225 ± 4 mm. If γ_{LV} is assumed to be 0.072 N/m, which is the surface tension of water [46], the effective contact angle θ between water and the capillary wall can be calculated to be 86°. This is definitely too high; the advancing contact angle between water and individual cellulose fibers reported in the literature is typically between 0 and 60° and the receding contact angle is 0 [6,16]. The static contact angles are determined by the equilibrium of interfacial energies whereas the dynamic contact angles depend on the unbalance of the local interfacial driving force and the viscous retarding force. This is another pitfall in applying the Washburn equation to a network of cellulose fibers. The microscopic variations in chemical composition, discontinuity, and roughness of the fiber surfaces are responsible for the local dynamic contact angle and give rise to diversity in spreading kinetics [3,47]. Furthermore, the tortuous pores in a fiber matrix are far from straight open capillaries. A more realistic model for water penetration into a fiber network can be constructed by introducing a tortuosity factor ξ, which is defined as the ratio between the actual distance which the meniscus travels in a given pore and the vertical distance measured as a straight line normal to the overall advancing front. If the equilibrium contact angle θ_e is assumed to be 0, from the curve fitting result h_∞, the tortuosity factor for the fiber matrix samples used in this investigation was roughly estimated to be about 14, which is a reasonable value for cellulose fiber matrices. The values of factor ξ for cellulose fiber samples reported in the literature [11,15] are between 12 and 23, which are determined from the ratios of the theoretical absorption coefficient of the cylindrical model to the observed absorption coefficient by Bristow method [15]. Equation (2) discussed

above is only an asymptotic solution for the capillary penetration problem based on a quasi-steady-state approximation. At short times, a more complete formulation of this problem is needed to take the kinetic energy and frictional work within the fluid into consideration. The more general and rigorous equation contains additional terms and has been discussed in the literature [3,48]. It has been reported that the inertial effects could affect the initial rate of the liquid imbibition into a porous medium. However, for long-time absorption experiments as in the present investigation, the deviations in the initial time period of the order of 1–100 ms are negligible.

The Washburn equation can quantitatively describe the time evolution of the advancing liquid front in a cellulose fiber matrix after introducing the tortuosity and effective pore radius concept. However, the Washburn equation predicts neither the uneven concentration distribution demonstrated in Fig. 3, nor the second concentration gradient boundary behind the leading liquid front shown in Fig. 4. The penetrating liquid in a porous fiber network follows the tortuous paths of different sizes. Besides the individual fiber-liquid interaction, the porous network structure of the absorbing medium also has a significant influence on the bulk absorbency performance of a fiber matrix. The kinetics of fluid flow in various porous systems is usually interpreted by using the empirical Darcy's law [49], which characterizes the flow in a porous medium in terms of the driving pressure head and the permeability of the medium. In the literature there are a number of models and empirical formulas available to correlate the structural and geometrical parameters of the porous medium (such as porosity, tortuosity, and specific surface area) with the permeability factor [1]. Darcy's law is usually considered applicable for a linear and steady laminar flow through a porous media. In practice, however, many absorbency processes occur in unsteady conditions where the distribution of the liquid saturation degree changes with time as clearly demonstrated in Figs. 3 and 4. The unsteady flow phenomenon in a porous medium is very similar to the concentration driving diffusion problem and can be adequately described by Darcy's equation in the differential form [1,49]

$$\frac{\partial s}{\partial t} = \frac{\partial}{\partial h}\left[F(s)\,\frac{\partial s}{\partial h}\right], \tag{3}$$

which relates the time variation of the saturation degree s to the distribution of the concentration gradient by the diffusivity factor, $F(s)$. Assuming a constant $F(s)$, Eq. (6) can be solved analytically,

$$s = 1 - \mathrm{erf}\left(\frac{h}{2\sqrt{Ft}}\right), \tag{4}$$

where erf(x) is the error function. Figure 5(a) shows the calculated concentration distribution as a function of time and liquid diffusion distance assuming a diffusivity value $F = 5\ \mathrm{mm}^2/\mathrm{s}$, which is in the range of values of cellulose fiber materials [1]. However, the NMR imaging data shown in Figs. 3 and 4 apparently do not validate such a simplification

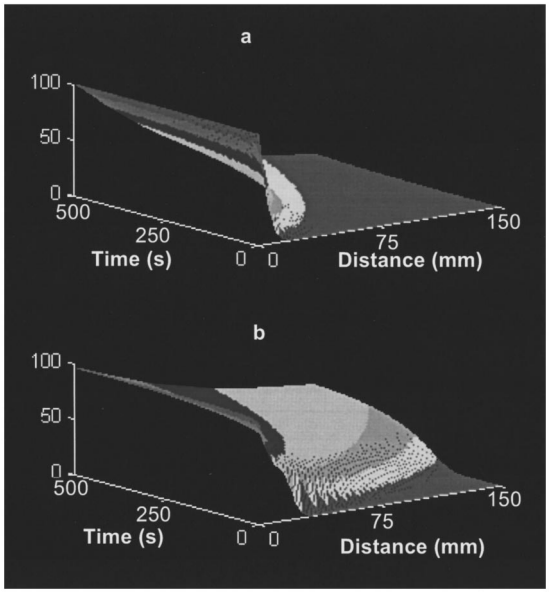

FIG. 5. Calculated saturation profiles based on Eqs. (4) and (6): (a) saturation profile due to concentration gradient driving diffusion process [Eq. (4)] and (b) a population-weighted sum of capillary penetration into pores between fibers and diffusion process into fibers.

as diffusion with constant diffusivity. This is expected since the advancing liquid front is not controlled by the water concentration gradient, but rather the capillary penetration process. Furthermore, diffusivity characterizing the diffusion process might be dependent on the distribution of the saturation degrees.

As indicated in the NMR imaging data (Figs. 3 and 4), the water imbibition into a fiber matrix consists of two different processes: capillary water flow between fibers and water diffusion into cellulose fibers. Both capillary flow and diffusion have to be taken into account in order to understand the change of water concentration distribution. Since the advancing liquid front in the fiber matrix samples follows the Washburn equation, the size of a filled capillary at a certain penetration height and time can be derived from Eq. (2). As indicated in Eq. (1), at fixed height, the larger pores fill first. The saturation degree s_p resulting from capillary penetration at a certain time and height should be equal to the volume fraction of filled pores relative to the total capillary pore volume, that is,

$$s_p(R) = \frac{\int_R^\infty P(R)R^2 dR}{\int_0^\infty P(R)R^2 dR}, \tag{5}$$

where $P(R)$ is the probability density distribution of the interfiber capillary pores of a fiber matrix sample. If the pore size distribution is assumed to be a Gaussian function with a mean pore size β and standard deviation α, it can be shown that

$$s_p(R) = \frac{\alpha(R+\beta)}{(\alpha^2+\beta^2)\sqrt{2\pi}} \exp\left[-\left(\frac{R-\beta^2}{2\alpha^2}\right)\right]$$

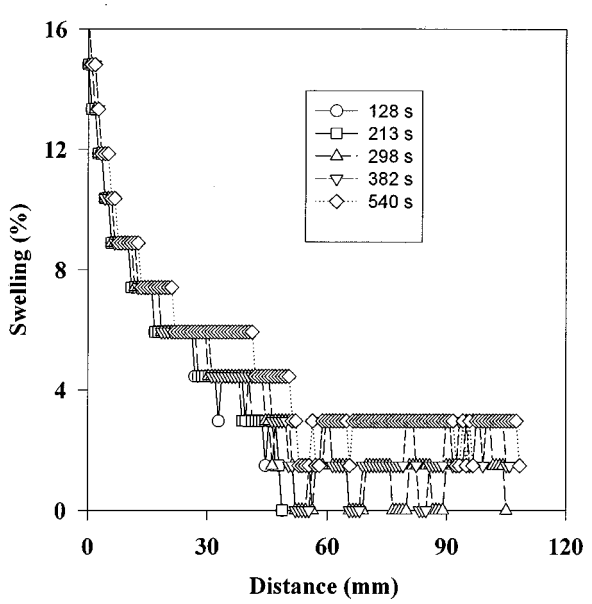

FIG. 6. Swelling degrees as a function of contact time and positions as measured from the dimensional changes of the wet fiber matrix relative to the original dry fiber plug.

$$+\frac{1}{2}\left[1-\mathrm{erf}\left(\frac{R-\beta}{\sqrt{2}\alpha}\right)\right]. \tag{6}$$

Since the interfiber capillary flow and the intrafiber water diffusion follow different time courses, the experimentally observed time evolution of the concentration profiles should be a population-weighted sum of both capillary penetration and intrafiber diffusion. Figure 5(b) shows results calculated from Eqs. (4) and (6) using a population ratio of 1:1. The contribution from the capillary flow was evaluated by assuming a Gaussian pore size distribution with a mean pore size β=4.3 μm and a standard deviation α=3 μm. The mean pore size used in the calculation is equal to the effective capillary radius estimated from the curve fitting of the Washburn equation and the value of standard deviation is also quite reasonable for cellulose fiber samples [11]. As shown in Fig. 2(b), the calculated results are qualitatively in accordance with the experimental data (Fig. 3). It appears that both interfiber capillary penetration and the intrafiber diffusion have to be taken into account in order to understand the time evolution of the water concentration distribution in a cellulose fiber matrix.

It is a well-documented phenomenon that water diffusion into cellulose fibers gives rise to cell wall swelling. This is also further evidenced by the NMR imaging data. Although NMR imaging cannot resolve individual fibers, the dimensional changes of fiber matrices accompanying the water imbibition are directly recorded by the dynamic water proton density images. The fiber swelling in a certain direction can, therefore, be calculated from the relative size increase of the wet fiber matrix relative the original dry sample. As shown in Fig. 6, the fiber swelling in the direction transverse to the capillary rise is significant during the long-time absorption experiment. Near the contacting liquid interface where the contacting time is longest, the fiber matrix swells up to 14%. The kinetics of swelling is controlled by the intrafiber diffusion mechanism. Cellulose fibers are mainly composed of cellulose macromolecules in ordered crystalline and disordered amorphous regions. When water penetrates into the amorphous regions, limited swelling of the cellulose fibers will occur. The swelling process stems from water diffusion into the space between cellulose macromolecules and can therefore be characterized by a diffusion coefficient [50,51]. Since the cellulose fiber wall structure can be regarded as concentric laminar capillaries, the specific surface area remains essentially constant, even when volumetric swelling occurs with increasing contact time. In the early days [7–13] capillary flow was considered to be the main mechanism for water to penetrate into fiber matrix. Wilson [7] proposed that diffusion processes might play an important part. Prise *et al.* [9] suggested that penetration could be divided into two stages: fast initial capillary flow and slower secondary penetration into fibers. This appears to agree with what was observed in the present study. Depending on the structure of the fiber matrix, the capillary penetration through the interfiber pores might be accompanied by a simultaneous diffusion process into the fiber.

SUMMARY AND CONCLUSIONS

The main advantages of dynamic spiral NMR imaging with self-refocusing rf pulse are the short slice selection duration and short overall data acquisition time. With the rapid dynamic spiral NMR imaging technique, it is possible to provide accurate measurements on the advancing water boundary, water concentration distribution, and swelling degree within the fiber matrix samples. The entire absorption process was continuously monitored as a function of time, and a synthesized image that shows the time evolution of the absorbed water concentration distribution within the fiber matrix was obtained from the entire NMR image data set. The NMR imaging data indicated that water imbibition into the fiber matrix consists of two different processes: water penetration into capillaries and water diffusion into cellulose fibers. The advancing liquid front is primarily determined by the water capillary flow and can be quantitatively described by the Washburn equation. The slower water diffusion process into fibers is mainly responsible for the fiber swelling. The time evolution of the absorbed water concentration distribution can be qualitatively interpreted in terms of a population-weighted sum of the capillary flow and the concentration-gradient-driven diffusion into fibers with a constant diffusivity. It is clear that the bulk absorbency performance of a fiber matrix are controlled by two factors: the individual fiber-liquid interaction and the porous network structure of the fiber matrix.

ACKNOWLEDGMENTS

Stimulating discussions with Professor L. Ödberg and Dr. T. Hindmarsh have been very helpful. We would like to acknowledge that this study is funded by the Swedish Research Council for Engineering Sciences.

[1] P. K. Chatterjee, *Absorbency* (Elsevier, Amsterdam, 1985).
[2] J. M. Drake and J. Klafter, Phys. Today **43**(5), 47 (1990).
[3] S. H. Wu, *Polymer Interface and Adhesion* (Dekker, New York, 1982).
[4] A. Borhan and K. K. Rugnta, J. Colloid Interf. Sci. **158**, 403 (1993).
[5] D. Danino and A. Marmur, J. Colloid Interf. Sci. **166**, 245 (1994).
[6] C. J. Nederveen, Tappi J. **77**, 174 (1994).
[7] W. S. Wilson, Paper Trade J. **126** (21), 45 (1948).
[8] H. Fujita, J. Phys. Chem. **56**, 625 (1952).
[9] D. Price, R. H. Osborn, and J. W. Davis, Tappi J. **36**, 42 (1953).
[10] R. Steele, Textile Res. J. **28**, 144 (1958).
[11] H. Yamazaki and Y. Munakata, in *Products of Papermaking*, edited by C. F. Baker (Pira Internation, Leatherhead, 1993), p. 913.
[12] J. Verhoeff, J. A. Hart, and W. Gallay, Pulp Paper Can. **64**, T509 (1967).
[13] E. T. Reaville and W. R. Hine, Tappi J. **50**, 262 (1967).
[14] J. A. Van den Akker and W. A. Wink, Tappi J. **52**, 2406 (1969).
[15] J. A. Bristow, Sven. Papperstidn. **70**, 623 (1967); **74**, 645 (1971).
[16] K. T. Hodgson and J. C. Berg, Wood Fiber Sci. **20**, 3 (1988).
[17] J. H. Klungness, Tappi J. **64**, 65 (1981).
[18] G. G. Allan and Y. G. Ko, Cellulose Chem. Technol. **29**, 479 (1995).
[19] A. Marmur, J. Colloid Interf. Sci. **124**, 301 (1988).
[20] A. Marmur, in *Modern Approach to Wettability: Theory and Applications*, edited by M. E. Schrader and G. Loeb (Plenum, New York, 1992), p. 327.
[21] J. Van Brakel and P. M. Heertjes, Nature (London) **254**, 585 (1975).
[22] K. S. Sorbie, Y. Z. Wu, and S. R. McDougall, J. Colloid Interface Sci. **174**, 289 (1995).
[23] R. Lucas, Kolloid Z. **23**, 15 (1918).
[24] E. W. Washburn, Phys. Rev. **17**, 273 (1921).
[25] S. Blackband and P. Mansfield, J. Phys. C **19**, L49 (1986).
[26] L. A. Weisenburger and J. L. Koenig, Appl. Spectrosc. **43**, 1117 (1989).
[27] L. A. Weisenberger and J. L. Koenig, Macromolecules **23**, 2445 (1990); **23**, 2454 (1990).
[28] T. P. L. Roberts, T. A. Carpenter, and L. D. Hall, J. Magn. Reson. **91**, 204 (1991).
[29] M. Ilg, J. Maier-Rosenkranz, W. Muller, K. Albert, and E. Bayer, J. Magn. Reson. **96**, 335 (1992).
[30] R. A. Grinsted and J. L. Koenig, Macromolecules **25**, 1229 (1992).
[31] P. Mansfield, R. Bowtell, and S. Blackband J. Magn. Reson. **99**, 507 (1992).
[32] Q. Wei, S. Yimin, and F. Lun, Chin. J. Polym. Sci. **11**, 358 (1993).
[33] G. D. Cody and R. E. Botto, Macromolecules **27**, 2607 (1994).
[34] M. Ilg, B. Pfleiderer, K. Albert, W. Rapp, and E. Bayer, Macromolecules **27**, 2778 (1994).
[35] M. Valtier, P. Tekely, L. Keine, and D. Canet, Macromolecules **28**, 4075 (1995).
[36] C. B. Ahn, J, H. Kim, and Z. H. Cho, IEEE Trans. Med. Imaging **MI-5**, 2 (1986).
[37] C. H. Meyer, B. S. Hu, D. G. Nishimura, and A. Macovski, Magn. Reson. Med. **28**, 202 (1992).
[38] D. G. Nishimura, P. Irarrazabal, and G. H. Meyer, Magn. Reson. Med. **33**, 549 (1995).
[39] H. Geen, S. Wimperis, and R. Freeman, J. Magn. Reson. **85**, 620 (1989).
[40] X. L. Wu, P. Xu, and R. Freeman, Magn. Reson. Med. **20**, 165 (1991).
[41] H. Geen and R. Freeman, J. Magn. Reson. **93**, 93 (1991).
[42] C. J. Hardy and H. E. Cline, J. Appl. Phys. **66**, 1513 (1989).
[43] A. Takahashi and T. Peters, Magn. Reson. Med. **34**, 446 (1995).
[44] C. H. Meyer, J. M. Pauly, A. Macovski, and D. G. Nishimura, Magn. Reson. Med. **15**, 287 (1990).
[45] P. T. Callaghan, *Principle of Nuclear Magnetic Resonance Microscopy* (Clarendon, Oxford, 1991).
[46] D. H. Kaelbe, *Physical Chemistry of Adhesion* (Wiley, New York, 1971).
[47] S. Newman, J. Colloid Interface Sci. **26**, 209 (1968).
[48] J. Szekly, A. W. Neumann, and Y. K. Chuang, J. Colloid Interface Sci. **35**, 273 (1977).
[49] J. Bear, *Dynamics of Fluids in Porous Media* (Dover, New York, 1988).
[50] T. Q. Li, U. Henriksson, T. Klason, and L. Odberg, J. Colloid Interface Sci. **154**, 305 (1992).
[51] T. Q. Li, U. Henriksson, and L. Odberg, J. Colloid Interf. Sci. **169**, 376 (1995).